PCCP

COMMUNICATION

View Article Online
View Journal | View Issue

Cite this: *Phys. Chem. Chem. Phys.*, 2023, **25**, 9031

Received 29th December 2022,
Accepted 7th March 2023

DOI: 10.1039/d2cp06064g

rsc.li/pccp

Well-dispersed Au co-catalyst deposited on a rutile TiO_2 photocatalyst *via* electron traps†

Tomoki Akiyama, Haruki Nagakawa and Tetsu Tatsuma *

We deposited Au nanoparticles as a co-catalyst onto a TiO_2 photocatalyst by reducing $[AuCl_4]^-$ using electrons trapped in the oxygen vacancies of TiO_2. The dispersibility and hydrogen production ability of the Au co-catalyst are higher than those prepared using the conventional photodeposition method.

Photocatalysis is attracting attention as a sustainable technology to drive redox reactions using solar energy and to harvest solar fuels. For semiconductor photocatalysts such as TiO_2,[1] it is essential to modify them with co-catalysts to achieve sufficiently high efficiencies.[2] For instance, noble metal nanoparticles deposited on an n-type semiconductor photocatalyst facilitate charge separation by accepting photo-excited electrons and promote cathodic reactions including multi-electron reactions such as hydrogen production from water.[3,4]

Various methods have been investigated for combining semiconductor photocatalysts with metal co-catalysts, including photodeposition (PD),[5] mechanical mixing[6] and impregnation methods.[7] Among these methods, the PD method is known to guarantee a good electrical contact between the metal and the semiconductor, leading to a high photocatalytic activity.[8] However, it is not necessarily easy to control the dispersibility of the co-catalyst nanoparticles using the PD method. This is because the deposition rate depends on the particle size and the crystal facets of the photocatalysts.[9] Furthermore, metal deposition should occur preferentially at the metal surface, which acts as the cathodic reaction site.[10] These effects lead to decreased dispersibility and monodispersity of the co-catalyst, which can in turn suppress the photocatalytic activity.

In the present study, we take advantage of electrons trapped at defect sites to improve the dispersibility of the co-catalyst. In the case of metal oxide photocatalysts, oxygen defects act as electron traps.[11] The energy-resolved distributions of the defect levels have been widely studied,[11–16] and the levels are found within the band gap region.[12,13] Under light irradiation, electrons in the valence band of the metal oxide are excited to the conduction band, and the excited electrons can be trapped by defect levels below the conduction band. If the excited electrons are trapped in relatively shallow levels, their lifetime can be prolonged, whereas electrons trapped by deep levels will be more likely to recombine with holes in the valence band.[17]

The electrons accumulated in electron traps can be used for the reductive deposition of metal nanoparticles, such as Ag, Pt, Au and Pd, onto semiconductor photocatalysts.[18–20] In this method, electrons are trapped in the defect levels under light irradiation, and reduction of the metal ions to metal nanoparticles occurs under dark conditions. Once a metal nanoparticle is deposited and the electrons trapped nearby are consumed in the deposition process, no further reduction reaction proceeds on the metal particle. Therefore, co-catalysts deposited by the trapped electrons can have a smaller particle size than those deposited using the PD method.[19,20] We also expect that this method will enable us to improve the dispersibility and monodispersity of metal nanoparticles. However, studies focusing on these aspects have not been reported so far. In addition, even though the metal co-catalysts are expected to reduce the overvoltage of the hydrogen evolution reaction, the co-catalysts deposited *via* the electron traps have been used primarily for the oxidative degradation of organic matter, and have not yet been applied to hydrogen production.[18–20]

In the present study, we employed a submicron-sized rutile TiO_2 photocatalyst and modified it with a Au co-catalyst using the electron trap-mediated deposition (ETD) method (Fig. 1a). The photocatalysts thus obtained were characterized in terms of their dispersibility, monodispersity and photocatalytic activity for hydrogen production, and were compared with the TiO_2 photocatalyst modified with Au *via* the PD method (Fig. 1b).

Rutile TiO_2 with a nominal average particle size of 200 nm (HT-0514, Toho Titanium) was dispersed in 50 vol% aqueous ethanol (10 g L^{-1}). The dispersion was purged with N_2 gas and sealed with a rubber cap, then irradiated with UV light for 10 min

Institute of Industrial Science, The University of Tokyo, Tokyo 153-8505, Japan. E-mail: tatsuma@iis.u-tokyo.ac.jp

† Electronic supplementary information (ESI) available: XRD and SEM data. See DOI: https://doi.org/10.1039/d2cp06064g

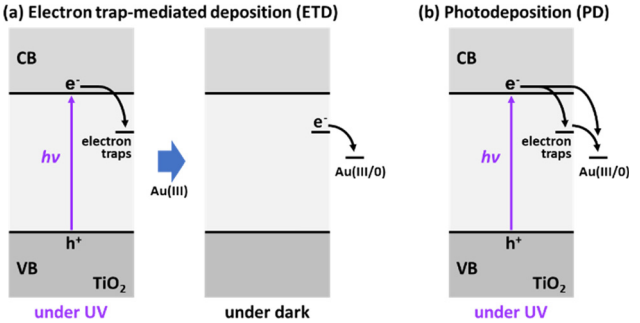

Fig. 1 Schematic illustration of the Au deposition processes *via* (a) the electron trap-mediated deposition (ETD) method and (b) the photodeposition (PD) method.

using an LED lamp (365 nm, ~500 mW cm^{-1}, Asahi Spectra) as a light source in order to accumulate electrons in the defect levels of TiO_2. The Au co-catalyst was then deposited by adding $H[AuCl_4]$ to the TiO_2 dispersion (5–100 μmol L^{-1}), while bubbling N_2 gas under dark conditions. Au–TiO_2 was also prepared using the PD method by simply irradiating the TiO_2 dispersion containing the same amount of $H[AuCl_4]$ with UV light for 10 min.

After UV irradiation in N_2-saturated aqueous ethanol for electron trapping in the ETD process, the absorption properties of TiO_2 were examined because the trapped electrons give a new absorption band in general.[11] A V-670 spectrophotometer (Jasco) with an integrating sphere was used to obtain the diffuse reflectance spectra shown in Fig. 2a. After light irradiation, the colour of the dispersion changed from white to blue, and a new absorption band appeared that covered the entire visible-light region (Fig. 2a). The defect levels in the band gap region accept electrons from the conduction band, and Ti^{4+} is reduced to Ti^{3+}. Excitation of the trapped electrons to the conduction band gives the broad visible absorption band.[21]

After the addition of $[AuCl_4]^-$ to the dispersion of TiO_2 with trapped electrons, the colour of the dispersion changed from blue to pink, and an absorption peak appeared around 540 nm (Fig. 2a), which is typical of the plasmonic absorption of Au nanoparticles. This indicates that the trapped electrons reduce $[AuCl_4]^-$ to metallic Au. The plasmonic peak was slightly red-shifted from the most commonly observed wavelength of 520 nm, probably because the Au nanoparticles were deposited on TiO_2 particles and the high refractive index of TiO_2 caused the red shift. Bridging oxygen species of rutile TiO_2 are known to be nucleation sites for metallic Au clusters[22–24] unless the surface is not hydroxylated,[25,26] and epitaxial growth to Au nanoparticles is possible at the (110) and (100) faces of rutile TiO_2.[27,28] In addition, once the oxygen vacancies are formed at the surface, the nucleation and growth processes are enhanced further.[22–24]

As the Au concentration in the growth solution was increased, the peak height for the Au–TiO_2 samples prepared using the PD method increased monotonically, indicating that the amount of deposited Au was increased (Fig. 2b). Incidentally, if the concentration was increased to 100 μmol L^{-1} or higher, signals of metallic Au appeared in the X-ray diffraction (XRD) patterns (Fig. S1, ESI†), although the Au nanoparticles

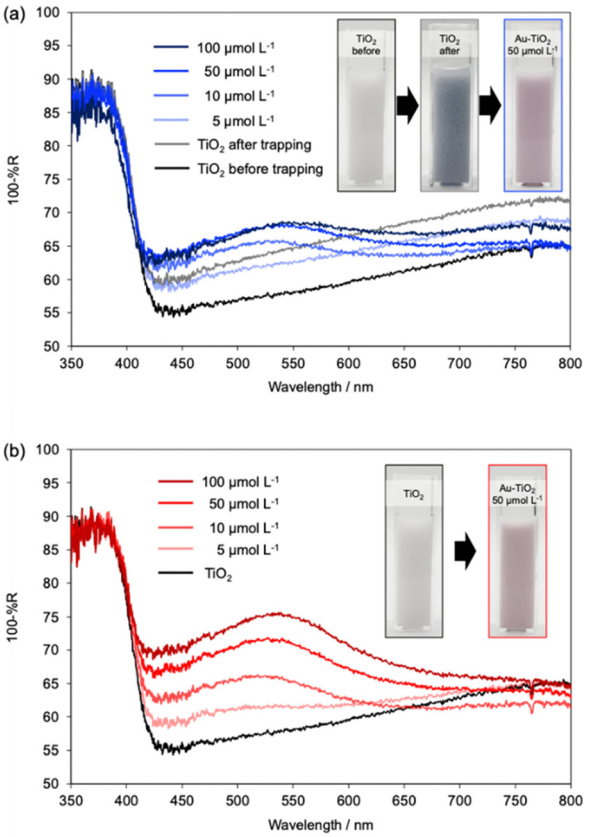

Fig. 2 (a) Diffuse reflectance spectra of suspensions of TiO_2 before and after the trapping of electrons at defect levels *via* UV irradiation for 10 min and spectral changes after the stepwise addition of $[AuCl_4]^-$ in the dark (ETD method). (b) Spectral changes during the stepwise addition (10 min each) of $[AuCl_4]^-$ under continuous UV irradiation (PD method). Insets show color changes of the suspensions in both processes.

were too small and too sparse to be detected at lower concentrations. By contrast, in the case of Au–TiO_2 samples prepared *via* the ETD method, the absorption due to the electron traps decreased gradually, while the plasmonic absorption peak of Au appeared (Fig. 2a). The peak height was increased at <50 μmol L^{-1}, but was almost saturated in the >50 μmol L^{-1} range.

These results indicate that the deposition amount is limited by the amount of Au in the solution at <50 μmol L^{-1}, and by the amount of trapped electrons at >50 μmol L^{-1}. At around 50 μmol L^{-1}, the total amount of Au seems to match the amount of trapped electrons. From the amount of $[AuCl_4]^-$ added to the reaction solution, the number of electrons required for reduction to metallic Au is calculated to be 15 μmol per g (TiO_2), considering that the reaction is one of three-electron reduction. This value is roughly consistent with the amount of electron traps of rutile TiO_2 used in this work (HT-0514), which is reported to be 23 μmol per g (TiO_2).[29] Incidentally, the slight red-shift of the plasmonic peak during the deposition process can be explained in terms of the slightly increased contact area between Au and TiO_2.

We also characterized the TiO_2 samples with the Au co-catalyst using scanning electron microscopy (SEM) and compared them with samples of TiO_2 before Au deposition (Fig. 3a–c). The Au

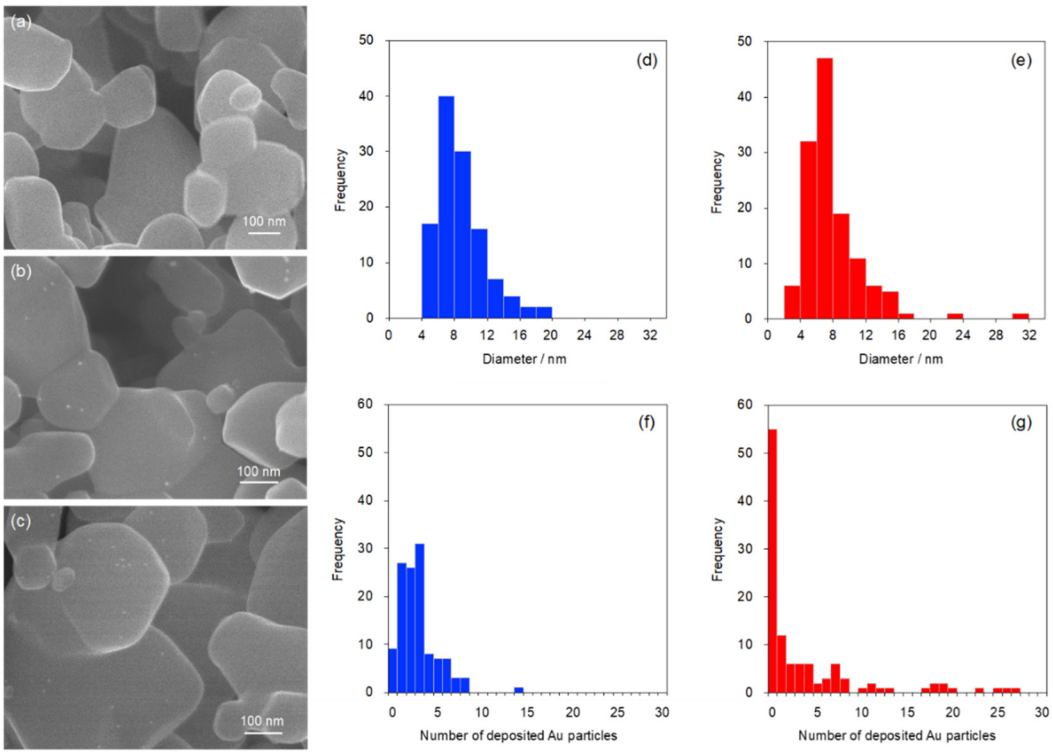

Fig. 3 SEM images of (a) TiO_2, (b) Au–TiO_2 prepared using the ETD method, and (c) Au–TiO_2 prepared using the PD method. Histograms (d and e) of the size of the Au nanoparticles and (f and g) the number of Au nanoparticles deposited on each TiO_2 particle measured and counted *via* SEM observation for the Au–TiO_2 samples prepared using the ETD (d and f) and PD (e and g) methods. The $[AuCl_4]^-$ concentration was 50 μmol L^{-1} in the deposition process.

co-catalyst was deposited in the presence of 50 μmol L^{-1} $[AuCl_4]^-$. Au nanoparticles were found on the TiO_2 surface for both of the samples prepared *via* the ETD and PD methods. Au nanoparticles are indicated with yellow arrows in Fig. S2 and S3 (ESI†) for each deposition method. To further corroborate that those were Au particles, we immobilized the Au–TiO_2 particles prepared *via* ETD and PD on an adhesive carbon tape and immersed it for 10 min in an aqueous solution containing 79 mmol L^{-1} I_2 and 60 mmol L^{-1} KI, in which Au is soluble. After this treatment, the small particles disappeared (Fig. S4 and S5, ESI†) and the plasmonic absorption peaks were suppressed almost completely, indicating that those small deposits were indeed Au nanoparticles. Histograms of the Au particle size are shown in Fig. 3d and e, and the average values of the particle size were 8.0 ± 4.0 nm and 8.8 ± 3.1 nm for the ETD and PD methods, respectively. Thus, there is no significant difference between the samples in terms of the monodispersity.

By contrast, there was a clear difference in the dispersibility of the Au co-catalyst. In order to quantitatively investigate the dispersibility, we counted the number of Au nanoparticles deposited on each TiO_2 particle in the SEM images. The results are shown as histograms in Fig. 3f and g, and the average numbers are 2.8 ± 2.1 and 3.8 ± 6.3 for the ETD and PD methods, respectively. It is clear that the statistical dispersion of the number for the PD method is greater than that for the ETD method. Of particular note is the number of TiO_2 particles without Au deposition, which is 7.4% and 48.2% of the all TiO_2 particles for the ETD and PD methods, respectively.

Such a difference in the dispersibility of the Au co-catalyst may affect the photocatalytic activity for hydrogen production. We therefore examined the activity in the presence of ethanol as an electron donor under UV light (365 nm). In the photocatalytic reactions, water molecules or protons are reduced to hydrogen by excited electrons in the conduction band, while ethanol is oxidized by the holes in the valence band. The amount of evolved hydrogen gas was evaluated using gas chromatography (490 Micro GC, Agilent Technologies). The hydrogen production rates were calculated from the slopes of the regression lines, which a showed high correlation ($R^2 > 0.99$) in the 0–40 min range (Fig. 4a). As a result, steady hydrogen production was observed for the TiO_2 samples with the Au co-catalyst, whereas the activity of that without Au was almost negligible. This means that the reaction was accelerated by the deposited reduction co-catalyst, which promoted either charge separation, reactant adsorption, electron transfer reaction or product desorption. Among the samples examined, the Au–TiO_2 sample prepared *via* ETD showed the highest hydrogen production activity, which was 2.5 times higher than that prepared using PD. Although Au–TiO_2 systems are known to show plasmon-induced charge separation[30] including hydrogen evolution from water,[31] the hydrogen production activity of the present photocatalysts was negligible, even under light that can excite the plasmons of Au nanoparticles.

We also prepared samples at different $[AuCl_4]^-$ concentrations, and their hydrogen production abilities are shown in Fig. 4b. As a result, all of the samples prepared *via* the ETD method showed higher activities than those of the PD method in the concentration range examined (5–100 μmol L^{-1}). The highest

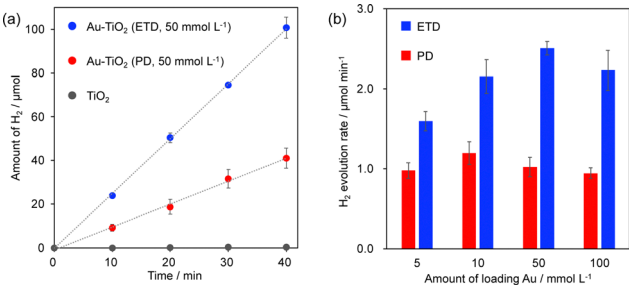

Fig. 4 (a) Time course of the amount of evolved hydrogen for the Au–TiO_2 samples prepared *via* the ETD and PD methods in the presence of 50 μmol L^{-1} $[AuCl_4]^-$ and for TiO_2 without Au. Each sample (50 mg) was suspended in a N_2-saturated aqueous solution (5 mL) containing 50 vol% ethanol and irradiated with UV light ($\lambda \approx 365$ nm). (b) Hydrogen production rate for the Au–TiO_2 samples prepared at different $[AuCl_4]^-$ concentrations. The error bars show the standard deviation values ($n = 3$).

hydrogen evolution rate of 2.5 μmol min^{-1} was observed at the $[AuCl_4]^-$ concentration of 50 μmol L^{-1} for the ETD method. By contrast, the optimum $[AuCl_4]^-$ concentration was 10 μmol L^{-1} for the PD method. Excess Au deposition during the PD method should decrease the photocatalytic activity through inhibiting the light absorption of TiO_2 and blocking oxidation reaction sites.[32] Since we used identical TiO_2 particles for both methods and there was no significant difference in the Au particle size, the factor affecting the activity should be the dispersibility of the Au co-catalyst. As mentioned above, the PD method gives many more Au-unloaded TiO_2 particles than the ETD method, and the unloaded particles show negligible activity for hydrogen production. We therefore conclude that the higher hydrogen production activity of the photocatalysts prepared *via* the ETD method is attributed to the higher dispersibility of the Au co-catalyst.

In conclusion, we successfully prepared Au–TiO_2 composites by taking advantage of the electron traps of TiO_2 using the ETD method, which gives a higher dispersibility of the Au co-catalyst than offered by the PD method. Since the amount of deposited Au is limited by the amount of electron traps for each TiO_2 particle, excess deposition can be avoided. The high dispersibility of the Au co-catalyst deposited using the ETD method leads to efficient photo-induced charge separation and a high photocatalytic hydrogen production activity. The Au–TiO_2 photocatalysis will be applied to other reactions, such as the oxidative removal of pollutants.

Conflicts of interest

There are no conflicts to declare.

Acknowledgements

This work was supported in part by a Grant-in-Aid for JSPS Fellows (JP22J00535 for HN) and a Grant-in-Aid for Scientific Research (A) (JP20H00325 for TT).

Notes and references

1 A. Fujishima and K. Honda, *Nature*, 1972, **238**, 37–38.
2 A. Fujishima, T. N. Rao and D. A. Tryk, *J. Photochem. Photobiol., C*, 2000, **1**, 1–21.
3 J. Yang, D. Wang, H. Han and C. Li, *Acc. Chem. Res.*, 2013, **46**, 1900–1909.
4 S. Trasatti, *J. Electroanal. Chem. Interfacial Electrochem.*, 1972, **39**, 163–184.
5 F. Möllers, H. J. Tolle and R. Memming, *J. Electrochem. Soc.*, 1974, **121**, 1160–1167.
6 T. Kawai and T. Sakata, *J. Chem. Soc., Chem. Commun.*, 1980, 694–695.
7 J. Disdier, J.-M. Herrmann and P. Pichat, *J. Chem. Soc., Faraday Trans. 1*, 1983, **79**, 651–660.
8 K. Wenderich and G. Mul, *Chem. Rev.*, 2016, **116**, 14587–14619.
9 M. C. Hidalgo, J. J. Murcia, J. A. Navío and G. Colón, *Appl. Catal., A*, 2011, **397**, 112–120.
10 M. Yamamoto, Y. Minoura, M. Akatsuka, S. Ogawa, S. Yagi, A. Yamamoto, H. Yoshida and T. Yoshida, *Phys. Chem. Chem. Phys.*, 2020, **22**, 8730–8738.
11 R. F. Howe and M. Gratzel, *J. Phys. Chem.*, 1985, **89**, 4495–4499.
12 S. Ikeda, N. Sugiyama, S. Murakami, H. Kominami, Y. Kera, H. Noguchi, K. Uosaki, T. Torimoto and B. Ohtani, *Phys. Chem. Chem. Phys.*, 2003, **5**, 778–783.
13 A. Nitta, M. Takase, M. Takashima, N. Murakami and B. Ohtani, *Chem. Commun.*, 2016, **52**, 12096–12099.
14 Y. Shen, A. Nitta, M. Takashima and B. Ohtani, *Chem. Lett.*, 2020, **50**, 80–83.
15 H. Nagakawa, T. Ochiai, H. Ma, C. Wang, X. Zhang, Y. Shen, M. Takashima, B. Ohtani and M. Nagata, *RSC Adv.*, 2020, **10**, 18496–18501.
16 H. Nagakawa and M. Nagata, *ACS Omega*, 2021, **6**, 4395–4400.
17 A. Yamakata, J. J. M. Vequizo and H. Matsunaga, *J. Phys. Chem. C*, 2015, **119**, 24538–24545.
18 X. Pan and Y.-J. Xu, *Appl. Catal., A*, 2013, **459**, 34–40.
19 T. Cai, Y. Liu, L. Wang, S. Zhang, J. Ma, W. Dong, Y. Zeng, J. Yuan, C. Liu and S. Luo, *ACS Appl. Mater. Interfaces*, 2018, **10**, 25350–25359.
20 H. Wu, W. Jiang, L. Shi, R. Li, L. Huang and C. Li, *iScience*, 2022, **25**, 103572.
21 Y. Yan, W. Shi, W. Peng, Y. Lin, C. Zhang, L. Li, Y. Sun, H. Ju, J. Zhu, W. Ma and J. Zhao, *Commun. Chem.*, 2019, **2**, 88.
22 E. Wahlström, N. Lopez, R. Schaub, P. Thostrup, A. Rønnau, C. Africh, E. Lægsgaard, J. K. Nørskov and F. Besenbacher, *Phys. Rev. Lett.*, 2003, **90**, 026101.
23 A. Vijay, G. Mills and H. Metiu, *J. Chem. Phys.*, 2003, **118**, 6536–6551.
24 D. Pillay and G. S. Hwang, *Phys. Rev. B: Condens. Matter Mater. Phys.*, 2005, **72**, 205422.
25 L. Shi, S. Meng, S. Jungsuttiwong, S. Namuangruk, Z.-H. Lu, L. Li, R. Zhang, G. Feng, S. Qing, Z. Gao and X. Yu, *Appl. Surf. Sci.*, 2020, **507**, 145162.

26 S. Hu, P. Wang, R. Gao, F. Bi and X.-R. Shi, *J. Mol. Model.*, 2023, **29**, 41.
27 H. Koga, K. Tada and M. Okumura, *Chem. Phys. Lett.*, 2014, **610–611**, 76–81.
28 E. Kazuma and T. Tatsuma, *Adv. Mater. Interfaces*, 2014, **1**, 1400066.
29 A. Nitta, PhD thesis, Hokkaido University, 2018.
30 Y. Tian and T. Tatsuma, *J. Am. Chem. Soc.*, 2005, **127**, 7632–7637.
31 A. Tanaka, S. Sakaguchi, K. Hashimoto and H. Kominami, *ACS Catal.*, 2013, **3**, 79–85.
32 S. Veziroglu, A.-L. Obermann, M. Ullrich, M. Hussain, M. Kamp, L. Kienle, T. Leißner, H.-G. Rubahn, O. Polonskyi, T. Strunskus, J. Fiutowski, M. Es-Souni, J. Adam, F. Faupel and O. C. Aktas, *ACS Appl. Mater. Interfaces*, 2020, **12**, 14983–14992.